Flexible robot-based in-line measurement system for high-precision optical surface inspection

Christopher Naverschnigg, Ernst Csencsics, and Georg Schitter, Senior Member, *IEEE*

***Abstract*—Advances in industrial manufacturing and an increasing trend towards direct integration of measurement systems in the production line require flexible, fast, precise and robust systems. This paper presents the development and evaluation of a fully automated robot-based in-line measurement system, suitable for applications incorporating process variability and uncertainty, however, requiring single micrometer resolution and low instrumentation effort. The system utilizes laser triangulation in combination with mechanical 2D-scanning for fast and precise measurements. Lissajous trajectories and a computer vision algorithm based on edge detection are used to locate relevant features within the scan area. This allows alignment of the measurement tool, by using plane fits, to optimally utilize the measurement range of the sensor system for a high resolution scan, applied to a refined area, providing robustness and flexibility. For a scan area of 25×25 mm the measurement uncertainty equals $6.4\,\mu$m at 2σ. The system accuracy is evaluated to $2.2\,\mu$m. The combined standard uncertainty of reference sample measurements equals $1.2\,\mu$m.**

***Index Terms*—Metrology, System Analysis and Design, Feature Detection, Manufacturing Automation, Automatic Optical Inspection**

I. Introduction

OVER the past decades, industrial manufacturing has faced significant challenges under the impact of global trends. Resource efficiency, mastery of new technologies, flexibility and transparency, have developed to be the primary focus of production lines. In addition, a continuing interest in the increase of manufacturing efficiency and product quality sets high demand on measurement systems and requires them to be integrated directly in the production line [1], [2]. In-line measurement eliminates steps such as unloading samples from the main assembly line, decreases the required time to detect problems within the manufacturing process, leads to a higher consistent throughput and enables the possibility of implementing statistical process control in order to identify equipment issues before they affect the final product [3]. Applications range from the automotive and aerospace sector to the semiconductor industry, where 3D-imaging and inspection systems are required to perform material characterization, defect detection and dimensional inspection [4], [5]. To fulfil these challenges, measurement systems are demanded to be flexible, fast, precise and robust.

The authors are with the Automation and Control Institute (ACIN), Technische Universität Wien, 1040 Vienna. Further author information: (Send correspondence to Christopher Naverschnigg)
Christopher Naverschnigg: E-mail: naverschnigg@acin.tuwien.ac.at, Telephone +43 (0)1 588 01-376 533

Flexibility within a large working volume can be provided by industrial robots with up to six degrees of freedom, which are indispensable in industrial manufacturing and are in combination with 3D measurement systems of growing importance for measurement tasks, e.g. the inspection of complex shapes and freeform surfaces [6].

Fast and precise imaging with high axial and lateral resolution is achieved by optical measurement systems, which are a preferred choice due to their non-tactile measurement principle [7]. The resolution of commonly used camera-based inspection systems, is proportional to the field of view and set by the camera system's design. Commercial stereo vision systems with a field of view of several millimeters, a lateral resolution down to $6.7\,\mu$m and an accuracy down to $6\,\mu$m are available [8] [9]. Maximum resolution can, however, only be achieved at the optimal operational distance [10]. To overcome these limitations and enable measurements with micro- down to sub-micrometer resolution for sample sizes, laser triangulation sensors or confocal sensors are used in combination with scanning systems [11]. Triangulation sensors are widely applied in quality inspection [12], especially in factories where ease of use and instrumentation costs are critical [13]. However, the resolution of systems, combining industrial robots and optical measurement systems, is limited due to the limited precision and accuracy of robots for paths and poses, which lies in the range of multiple tens of micrometers [14], [15]. A robotic scanning system utilizing triangulation sensors mounted directly on the robot flange achieves a resolution down to $50\,\mu$m after a calibration process [16]. Other reported or commercially available robot-based systems integrating triangulation line sensors [17], MEMS-based scanners [18], galvanometric scanners [19] and stereo vision [20], achieve an accuracy limited to several tens of micrometer, which is insufficient for numerous applications requiring measurements on the single micrometre scale. For high precision applications with sub-micrometer resolution, a measurement platform as robotic end effector has been reported in combination with an optically scanned 3D sensor [21], [22]. The system is, however, subject to a significant instrumentation effort and has a limited scan area of only $100\,\mu$m, making it impractical for applications with process variability and uncertainties in the millimeter range [23], [24].

These inaccuracies lead to an inefficient measurement process and can increase the measurement time significantly. To compensate for process uncertainties and locate relevant features, additional vision-guided systems can be employed for online position correction and path planning [25]. Using reference markers of model reconstruction from point-cloud

Post-print version of the article: C. Naverschnigg, E. Csencsics, and G. Schitter, "Flexible Robot-Based In-Line Measurement System for High-Precision Optical Surface Inspection," *IEEE Transactions on Instrumentation and Measurement*, vol. 71, 2022. DOI: 10.1109/TIM.2022.3216680

data, they often require a sample modification, provide only accuracies in the millimeter range and again increase the instrumentation effort and cost [26].

The contribution of this paper is the integrated design and evaluation of a versatile robot-based in-line measurement system for 3D surface inspection providing single micrometer resolution, a low instrumentation effort and a large measurement area with the capability to alleviate process and alignment uncertainties by intelligent system operation. The integrated measurement system design is centred around a dual-stage actuation concept and an optimized dual-scan approach enabling an online alignment correction and feature detection as well as an efficient measurement process. It is further designed for accommodating various compact optical sensors based on different principles, making it applicable to a plethora of measurement tasks.

The remainder of the paper is structured as follows: (II) system design and prototype implementation of the measurement system, (III) methods for intelligent operation and improved performance, (IV) experimental validation, (V) conclusion.

II. Robotic high-precision in-line measurement system

A. System requirements

The requirements are evaluated based on the overall goal of creating a fast and flexible, but simultaneously precise and robust in-line measurement system for surface inspection, e.g. for the inspection of complex parts and surface structures in the automotive and aerospace sector, such as weld spots and weld seams. This requires the system to be positioned within a large working volume with dimensions up to several meters. A lateral and axial measurement range of multiple tens of millimeters is demanded to cover a wide range of object shapes, to provide flexibility for different features sizes and to deal with uncertainties of the feature location. A measurement volume of at least $25\,\mathrm{mm} \times 25\,\mathrm{mm} \times 25\,\mathrm{mm}$ is desirable.

Simultaneously, fast and high-precision measurements for dimensional inspection and characterization of surface properties (e.g. cracks, porosity) are desired, which requires micrometer to sub-micrometer axial resolution. A lateral resolution of at least $100\,\mu\mathrm{m}$ is demanded.

With typical spot weld diameters ranging from 3-7 mm [27], for a measurement area of $5\,\mathrm{mm} \times 5\,\mathrm{mm}$, a maximum measurement time of $3\,\mathrm{s}$ is targeted to provide reasonable throughput. The specifications are summarized in Table I.

TABLE I
System requirements

Property	Value	
Measurement volume	$> 25 \times 25 \times 25$	mm
Axial resolution	< 1	μm
Lateral resolution	< 100	μm
Maximum measurement-time for 5×5 mm	3	s

B. System design

The system design is illustrated in Figure 1. To fulfil the requirements regarding resolution, measurement range and to provide high versatility for different materials, a single point laser triangulation sensor is used which requires an additional positioning system to perform a high-precision scan movement.

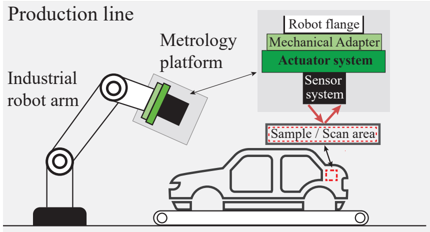

Fig. 1. Robot-based in-line measurement system for surface and material inspection.

For flexible inspection within the production line a 6-DOF industrial robot is considered. Whereas industrial robots can achieve position accuracy and repeatability in the range of multiple tens of micrometers, their ability to follow a path or trajectory is often lowered by a factor of ten. Therefore, an industrial robot is not suitable for performing a high-precision scan movement. An additional actuator system is necessary to combine flexible orientation of the measurement tool in a large working volume with the task of high-precision optical surface inspection. This results in a dual-stage approach.

The main tasks of the additional actuator system are point-to-point movements with high positioning accuracy and repeatability to minimize lateral error, or the tracking of a scan-trajectory with desired acceleration and velocity. The requirements regarding scan time and lateral resolution lead to minimum velocity and acceleration of $100\,\mathrm{mm/s}$ and $10\,\mathrm{m/s^2}$ of a raster trajectory. Linear actuators, in terms of either voice-coil actuators or stepper-motor-based stages, are an appropriate choice, since they provide a range of motion of multiple tens to hundreds of millimeters and velocities of the carriage beyond several $100\,\mathrm{mm/s}$. The downside of voice-coil actuators is their relatively low force to current ratio compared to their weight and construction size. Stepper motor-based stages can provide high forces of multiple tens of Newton and provide a compact design while being able to keep up with micrometer precision, suitable for this application. Furthermore, due to the high forces, they support higher robot joint accelerations and velocities without the need for an additional locking mechanism to protect the carriage and the attached sensor system.

A two-dimensional scanning motion can be achieved by a single xy-actuator that provides a two-axis movement or two separate stacked linear stages. A single xy-actuator typically requires a more robust mechanical frame which leads to an increase of the total mass. This can lead to a mass of multiple kg for a robust design [28], which might exceed the load capacity of a compact industrial robot arm. Compared to single-axis linear stages, they typically also offer lower maximum

Post-print version of the article: C. Naverschnigg, E. Csencsics, and G. Schitter, “Flexible Robot-Based In-Line Measurement System for High-Precision Optical Surface Inspection,” *IEEE Transactions on Instrumentation and Measurement*, vol. 71, 2022. DOI: 10.1109/TIM.2022.3216680

velocities [29]. To minimize the applied load onto the robot arm and provide maximum scan speed, a xy-scan system based on two stacked single-axis linear stages is chosen.

C. Prototype implementation

A prototype of the robot-based in-line measurement system for optical surface inspection is created based on the system design choices and is shown in Figure 2. The system utilizes a six-degree-of-freedom industrial robot arm (IRB120, ABB AG, Sweden/Switzerland). The robot has a range of motion of $0.58\,\mathrm{m}$ and a load capacity of $3\,\mathrm{kg}$. Position accuracy and repeatability according to the datasheet are equal to $20\,\mu\mathrm{m}$ and $10\,\mu\mathrm{m}$. Regarding linear paths, the accuracy and repeatability lie in a range of 7-16 $\mu\mathrm{m}$ and 21-38 $\mu\mathrm{m}$ respectively. These specifications, especially when considering a scan movement, once again show, that the robot itself is not suitable for performing precision measurement tasks in the single micrometer range.

The robot arm is equipped with two stepper motor based linear stages (LSM050BE03T4, Zaber Technologies Inc., Canada). The stages are stacked and serve as a xy-scan system with a maximum speed of $120\,\mathrm{mm/s}$, a travel range of $50\,\mathrm{mm}$ and a peak thrust of $25\,\mathrm{N}$. Accuracy and repeatability result to $0.36\,\mu\mathrm{m}$ and $1.37\,\mu\mathrm{m}$.

The positioning system is equipped with a class 2 laser triangulation sensor (ILD1420-25, Micro-Epsilon Messtechnik GmbH & Co. KG, Germany). The sensor has a measurement range of $25\,\mathrm{mm}$, a minimum laser spot size of $55\,\mu\mathrm{m} \times 50\,\mu\mathrm{m}$ and an axial resolution of $0.385\,\mu\mathrm{m}$. The measurement sample rate is $4\,\mathrm{ksps}$, resulting in a short illumination time, which lowers the impact of motion blur, during a high speed scanning motion. 3D-printed adapters are designed to combine components and ease accessibility of the sample relative to the sensor system. A summary of the components' specifications is listed in Table II.

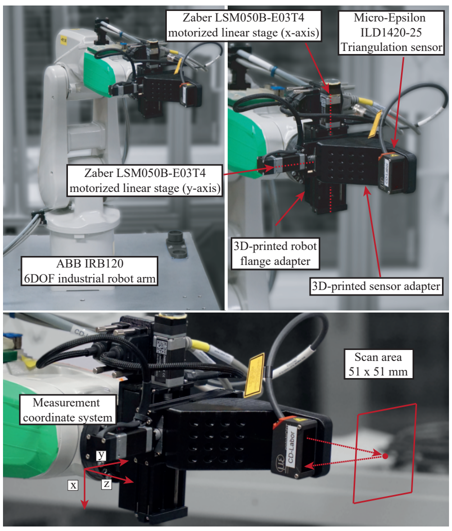

Fig. 2. Overview of the prototype setup utilizing a stepper-motor based xy-scan system and a triangulation sensor, mounted on an industrial robot arm.

TABLE II
COMPONENT SPECIFICATION OVERVIEW

Component	Specification	Value	
Robot arm	Pose accuracy	0.02	mm
	Pose repeatability	0.01	mm
	Maximum range	580	mm
	Load capacity	3	kg
Linear stage	Travel range	51	mm
	Accuracy	0.36	μm
	Repeatability	1.37	μm
	Maximum velocity	120	mm/s
	Maximum force	25	N
Triangulation sensor	Measurement range	25	mm
	Resolution	0.385	μm
	Repeatability	1	μm
	Minimum spot size	55×50	μm

The system's components are interfaced via modules by Beckhoff Automation, which are communicating via EtherCAT, allowing integration in existing industrial processes. An EtherCAT-Coupler is connected to a PC and the system is programmed using the TWINCAT3-Software (Beckhoff Automation, Germany). Scan data is automatically transmitted to Matlab, using the device and fieldbus-independent ADS interface provided by Beckhoff Automation, which performs the data processing. A socket for communication between Matlab and the robot control is implemented to exchange data, send commands and subsequently adjust the robot pose.

III. Scan and Measurement Process

An intelligent scan and measurement process is implemented to reduce the overall measurement time, increase robustness by compensating for potential feature deviations in a production line and to maximize the scan resolution. Relevant features are located during a coarse scan by using appropriate trajectories. The data of the initial scan is used to determine the orientation of the sample surface by using plane fits, which enables the adjustment of the robot pose for optimal utilization of the measurement range of the triangulation sensor. A high-resolution raster scan is applied to the refined area where the feature is located, in order to provide the required level of detail. For the high-resolution scan a raster trajectory is used to provide equal spatial resolution and to minimize scan time.

A. Lissajous-based scanning for fast overview

Recently attention has been shifted to Lissajous trajectories as an alternative to classic raster scans [30]. Compared to raster scans they provide a fast overview of the entire scan area. This property can be utilized to efficiently detect features within a small proportion of the total scan duration.

Lissajous trajectories are created by performing sinusoidal movements with different frequency in orthogonal scan directions. To select suitable frequency combinations for a desired scan area and expected features size, an integer constrained optimization problem is solved [31], with the goal of minimization of scan time and constraining resolution, quantified by using Voronoi tessellation [32]. This method is selected to constrain the number of decimal digits of frequencies, avoiding resolution calculation for combinations which lead

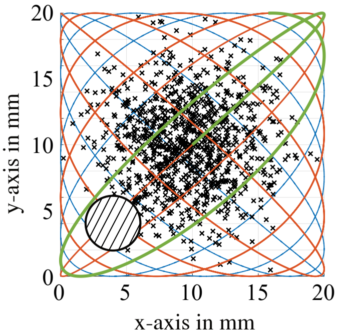

Fig. 3. Feature localisation using raster and Lissajous trajectories. Average proportion (green line) and maximum proportion (red line) of Lissajous trajectory (blue line) required to detect a feature with normal distributed position deviation.

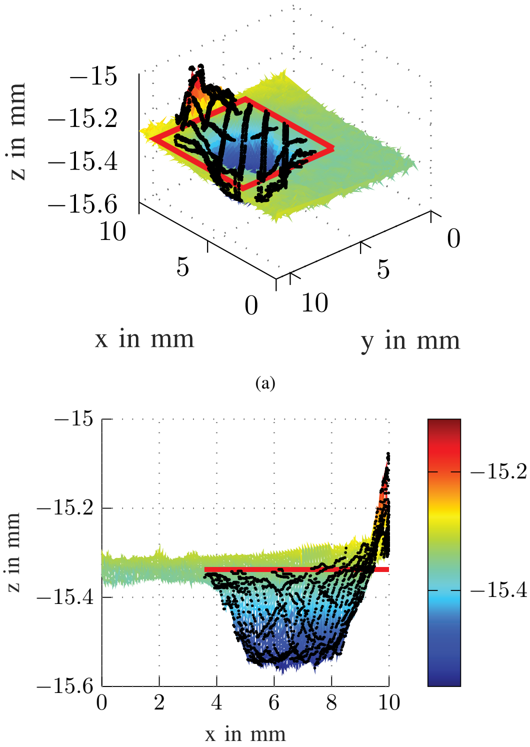

(a)

(b)

Fig. 4. Feature localization based on Lissajous scan data. (a) Scan data and detected edges (marked by black dots) of a weld spot and its surrounding area, (b) xz-view.

to high duration for poor initial conditions, hereby reducing computational effort. The maximum time to detect a feature of a certain size depends on the area, in which the feature is to be expected, since the maximum velocity of the linear stages limits the motion speed. Initial scan area and estimated feature size can be defined by using a-priori information of the process.

By assuming a normal distributed sample position of a circular feature with a diameter of $4\,\mathrm{mm}$ around the centre point in an area of $20\,\mathrm{mm} \times 20\,\mathrm{mm}$, with a standard deviation of 1/6 of the area width, as shown in Figure 3, an average time of $0.75\,\mathrm{s}$ is required to locate the feature. The green and red line mark the average and the maximum proportion of the trajectory that is required for 1000 normally distributed locations. If the area can be reduced to $10\,\mathrm{mm} \times 10\,\mathrm{mm}$, due to a decreased location uncertainty, and the Lissajous trajectory is adjusted accordingly, the average time is for example reduced to $0.15\,\mathrm{s}$. Since the scan time is proportional to the area size, the overall scan time is strongly reduced, if a high resolution scan is restricted to the region of interest, in which the features is detected. This is particularly relevant for the case with a large uncertainty but high resolution demands. For example, a raster scan with a resolution of $50\,\mu\mathrm{m}$, a velocity and acceleration of $120\,\mathrm{mm/s}$ and $10\,\mathrm{m/s^2}$ of the linear stages, requires a scan time of $\sim 71.5\,\mathrm{s}$ for an area of $20\,\mathrm{mm} \times 20\,\mathrm{mm}$. A scan, with equal resolution of a $4\,\mathrm{mm} \times 4\,\mathrm{mm}$ area, however, only requires $\sim 3.6\,\mathrm{s}$.

B. Feature localization for increased robustness

To allow the detection of features during a coarse pre-scan, a form of Canny edge detection is implemented [33]. In the first step, the image is smoothed by applying a Gauss-filter to remove noise and reduce the impact of outliers. The strength of the filter is defined by the standard deviation σ of the Gaussian distribution. The window size is selected depending on the standard deviation. A higher standard deviation leads to a bigger window which results in stronger smoothing and noise suppression. Afterwards, the Sobel operator is applied by convoluting the image and the operator to calculate the derivative for both, x and y direction. The Sobel operator is defined by the following matrices (1) [34]:

$$Gx = \begin{bmatrix} -1 & 0 & 1 \\ -2 & 0 & 2 \\ -1 & 0 & 1 \end{bmatrix}, \qquad Gy = \begin{bmatrix} -1 & -2 & -1 \\ 0 & 0 & 0 \\ 1 & 2 & 1 \end{bmatrix} \tag{1}$$

Figure 4 shows the scan data of a spot weld and its surrounding area. The area is scanned by using a coarse Lissajous scan. The red square marks the area in which the feature is detected and used for a high-resolution raster scan. After the fine scan, both datasets are combined which leads to Figure 4a. Figure 4b shows a perspective view of the xz-plane.

C. Robot pose adjustment for increased resolution

The data from the coarse scan is used to align the measurement system in optimal distance and orientation immediately after the detection process is finished. For parallel alignment of measurement and sample plane, a dominant plane within the measurement area is determined by using a plane fitting approach. As a basic least-squares algorithm can lead to ambiguous results if multiple dominant planes are present within the measurement area [34], a RANSAC algorithm is implemented [35]. Figure 5a shows the result when performing

Post-print version of the article: C. Naverschnigg, E. Csencsics, and G. Schitter, “Flexible Robot-Based In-Line Measurement System for High-Precision Optical Surface Inspection,” *IEEE Transactions on Instrumentation and Measurement*, vol. 71, 2022. DOI: 10.1109/TIM.2022.3216680

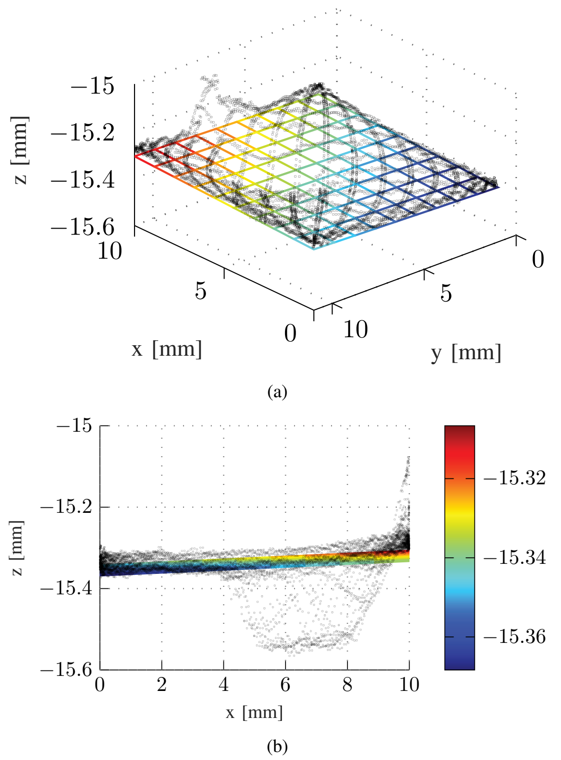

Fig. 5. Coarse Lissajous scan of a spot weld and plane fit for optimal alignment. (a) Scan data and plane fit (sample points marked by black dots), (b) xy-view.

plane fits for the coarse scan data from the previous section (cf. Figure 4). Figure 5b shows the xy-view of data points and fit. Data points acquired along the Lissajous scan are marked by black dots. After the fit, the plane model is used to calculate translation and orientation with respect to the robot arm. The position, of the end-effector (tool-centre-point) is defined by a vector containing xyz coordinates for the translational part. In contrast, the orientation is defined using quaternions which simplifies mathematical operations compared to the usage of rotation matrices, e.g. when using Euler-angle convention [36]. The resulting data can also be used to characterize the diameter of the weld spot and the indentation depth, which servers as a quality measure. This weld spot shows a diameter of approximately $4.45\,\mathrm{mm}$ and a maximum indentation of $194\,\mu\mathrm{m}$. According to DIN EN ISO 18595:2021 [37], the indentation depth must no exceed $20\,\%$ of the thickness of one sheet metal. For a sheet thickness of the sample of $1\,\mathrm{mm}$ this weld spot fulfils the criteria. The elevation next to the welding spot results from residuals of the welding process. Furthermore, the weld spot does not show surface cracks or porosity.

IV. Experimental results

A. System verification

The performance of the system is evaluated in accordance with ”The Guide to the Expression of Uncertainty in Measurement (GUM)” to determine the total measurement uncertainty, and to give an estimation on the system's accuracy by means of standard uncertainty [38]. In general, Type A standard uncertainty u, representing the standard deviation of the mean of a series of observations z_j, is calculated as follows

$$u(\overline{z}) = \frac{\sigma(z_j)}{\sqrt{n}}, \tag{2}$$

with standard deviation σ and number of observations n. For repeated surface measurements each series of measurement points, for the same xy-position is considered to have an individual u and σ [39]. The mean is calculated for determination of the overall standard uncertainty and standard deviation to extend the concept for surface measurements.

A reference sample with structures and step heights of $100\,\mu\mathrm{m}$ and an area of $25\,\mathrm{mm} \times 25\,\mathrm{mm}$ is selected as target. A raster scan of a coordinate-measuring-machine (CMM), which performs optical inspection using a confocal chromatic sensor, is carried out with a step size of $50\,\mu\mathrm{m}$ to provide a reference measurement [40]. The result is shown in Figure 6a. In prior, the standard uncertainty of the CMM is evaluated as described by conducing 20 line measurements with a step size of $50\,\mu\mathrm{m}$. The average standard uncertainty is $0.4\,\mu\mathrm{m}$.

The robot-based measurement system is assigned to carry out ten validation measurements of the reference sample. To limit the impact of high-acceleration forces on the mechanical structure, especially at turning points, the maximum acceleration of the linear stages is set to $500\,\mathrm{mm/s^2}$. This results in a maximum velocity of $111.8\,\mathrm{mm/s}$ at the centre of the stage and a scan time of $223.5\,\mathrm{s}$, for a raster scan with 500 lines. The result is shown in Figure 6b. Reference and validation measurements results from systems referenced to different coordinate systems. Therefore, grid, spacing and orientation of the data points is not identical. To directly compare both measurements during error calculation, the data sets have to be registered. Point cloud registration is carried out by using an iterative-closest-points (ICP) algorithm [41]. To calculate the deviation between the two datasets, data points, which lead to a minimization of the euclidean distance within the xy-plane, are matched with each other using a k-nearest-neighbour- (KNN-) algorithm [42].

To estimate the accuracy in z, at first the average error in height variations of all structures is calculated individually. Afterwards an overall mean value for the error is calculated. Individual consideration of constant height areas lead to a more general representation resulting in an overall mean value of $2.1\,\mu\mathrm{m}$. To give an estimation on how accurate the mean value is, the standard uncertainty is calculated. Standard uncertainty and standard deviation are evaluated by only using the data of the validation measurements. The standard uncertainty for ten measurements is found to be $1.1\,\mu\mathrm{m}$. The combined standard uncertainty of CMM and robot-based measurement system is calculated by the square root of the sum of squares, and equals $1.2\,\mu\mathrm{m}$. With a coverage factor of 2 for the expanded uncertainty, representing a confidence of approximately $95\,\%$ in the case of a normal distribution, each axial measurement is equal to $\pm 2.4\,\mu\mathrm{m}$. For a measurement range of $25\,\mathrm{mm}$ the relative standard uncertainty equals $0.005\,\%$. The overall

Post-print version of the article: C. Naverschnigg, E. Csencsics, and G. Schitter, “Flexible Robot-Based In-Line Measurement System for High-Precision Optical Surface Inspection,” *IEEE Transactions on Instrumentation and Measurement*, vol. 71, 2022. DOI: 10.1109/TIM.2022.3216680

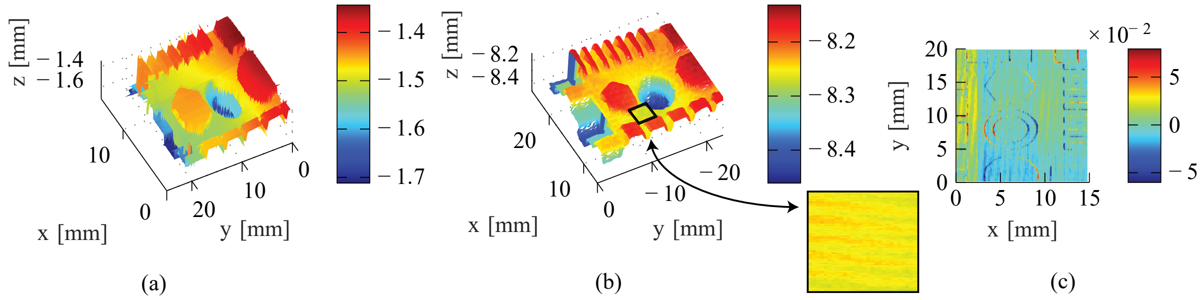

Fig. 6. Measurement of sample structures. (a) Reference measurement with a lateral resolution of 50 μm, (b) Validation measurement with a lateral resolution of 50 μm in x using the proposed measurement system, (c) axial error.

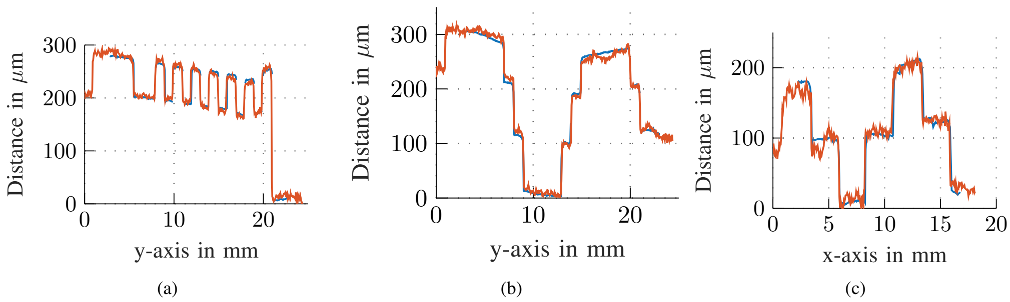

Fig. 7. Cross sections of sample structures. Comparison of CMM (blue) and robot-based measurement system (red) showing good agreement of the measurement results. (a) yz-plane, $x = 12$ mm, (b) yz-plane, $x = 6$ mm, (c) xz-plane, $y = 19$ mm.

uncertainty of the measurement is equal to 6.4 μm at two times the standard deviation. A summary of the achieved specifications is given in Table IV.

Mean absolute error $\bar{e}$ and error standard deviation σ_e are calculated for the matched samples individually. The axial error is shown in Figure 6c. The borders of structures indicate an error due to a remaining misalignment of the data of the registration process, however, these errors are neglected for error calculation. This results in a mean absolute error of 4.4 μm with a standard deviation of 3.2 μm. Figure 7 shows the comparison of cross-sections through the yz- and xz-plane. A summary is given in Table III.

Uncertainty of the measurement is affected by random errors, e.g. sensor noise and robot vibrations. In addition, the data of the validation measurement shows a periodic pattern, illustrated in the insert of Figure 6b. It is not visible in the CMM-scan and a rotation of the sample between two scan processes proves that this pattern must be associated with the scanning system. This effect is considered to result from a combination of straightness, flatness and Abbe error the linear stages. Furthermore a spatial shift of the pattern during operation might occur due to backlash, thermal expansion and starting point of the scan however, this dominant error component is expected to be reduced by a calibration procedure.

B. Optimal alignment for increased performance

In this section the impact of the repositioning process on the high-resolution scan is investigated. In Figure 8a the

TABLE III
ERROR EVALUATION FOR TEN SURFACE MEASUREMENTS UNDER EQUAL ENVIRONMENTAL CONDITIONS.

	Mean absolute error $\bar{e}$, μm	Error standard deviation σ_e, μm
Cross section		
x=12 mm, Figure 7a	2.7	6.1
x=6 mm, Figure 7b	3.5	5.4
y=19 mm, Figure 7c	6.2	4.3
Area		
25 mm × 25 mm	4.4	3.2

TABLE IV
SYSTEM SPECIFICATIONS IN AXIAL DIRECTION.

Robot-based measurement system	Accuracy	2.2	μm
	Standard uncertainty	1.1	μm
	Uncertainty at 2σ	6.4	μm
	Mean absolute error	4.4	μm
CMM	Standard uncertainty	0.4	μm

measurement system is only coarsely positioned with respect to the sample, such that the sensor is in range and the sample is measured without utilizing the repositioning feature. In Figure 8b, a coarse Lissajous scan is performed, followed by a plane fit utilizing a RANSAC algorithm. The optimal sensor distance is defined according to the point of minimal spot diameter specified in the datasheet, which is equal to a distance of 6 mm. The resulting plane parameters are used to calculate a new position of the robot arm for the high-resolution scan.

Post-print version of the article: C. Naverschnigg, E. Csencsics, and G. Schitter, "Flexible Robot-Based In-Line Measurement System for High-Precision Optical Surface Inspection," *IEEE Transactions on Instrumentation and Measurement*, vol. 71, 2022. DOI: 10.1109/TIM.2022.3216680

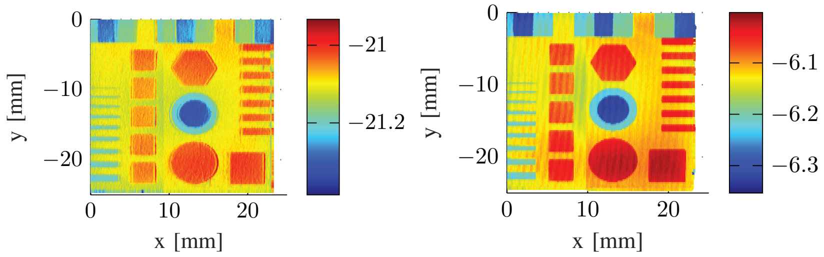

(a) (b)

Fig. 8. Results with and without optimal alignment, (a) non-optimal alignment, $\bar{e} = 6.3\,\mu$m, (b) optimal alignment showing improvement of the measurement result, $\bar{e} = 4.4\,\mu$m.

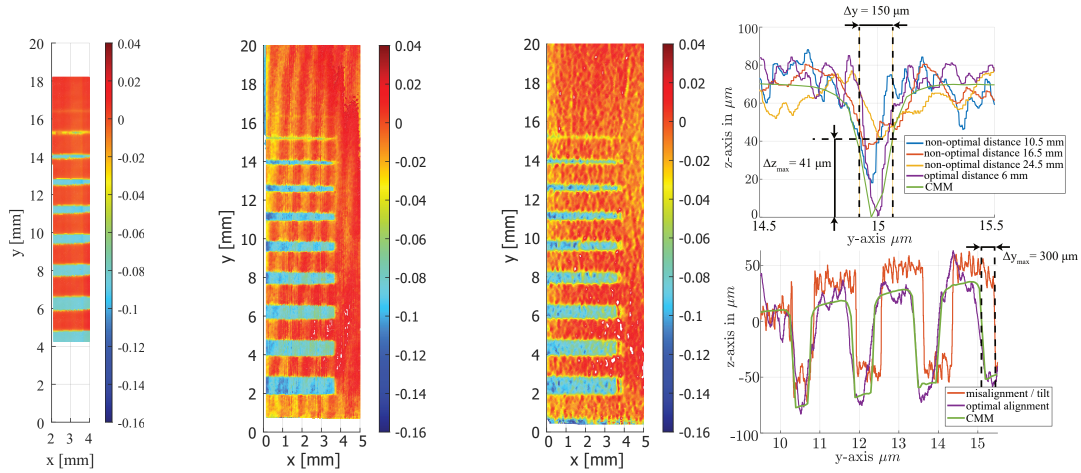

(a) (b) (c) (d)

Fig. 9. Comparison and improvement by robot pose adjustment. (a) reference measurement, (b) optimal alignment, (c) non-optimal alignment, (d) comparison for mean distance to sample variation (top) and misalignment due to a 5 degree tilt of the sample xy-plane.

The lateral resolution is proportional to the spot diameter on the surface. Therefore, a deterioration of the lateral resolution is expected to occur if the sensor is positioned in non-optimal distance. The result shows a lower distinction and sharpness of edges, as well as a blurred appearance. The sample structures partly also show doubled edges that are expected to be a consequence of the larger spot diameter. By calculating the error between the CMM-scan and the scan in the optimal and non-optimal distance for 10 measurements each as described in Section IV-A, the overall error is found to be reduced by approximately 30 % if the measurement system is positioned in optimal distance from $\bar{e} = 6.3\,\mu$m to $\bar{e} = 4.4\,\mu$m. Figure 9 shows the scan result for the section of the sample with the smallest structures. Figure 9a shows the result of the reference measurement. Figure 9b shows the result with optimal alignment. Similar to Figure 8a it can be seen that the CMM-scan and the scan in the optimal distance and orientation show a sharp delineation of edges. Figure Figure 9c shows the scan result for non-optimal alignment. The scan in the non-ideal distance shows a blurred appearance, and degradation of lateral resolution can be observed. Figure 9d (top) shows a sectional view of the smallest indentations of the reference sample with a width of 150 μm for a variation of the mean distance to the sample. The indentations at y = 15.1 mm shows a depth of 66 μm according to the reference scan. The indentations are clearly visible in the scan result. The measured indentation depth for optimal alignment is in good agreement with the reference scan. For an increased distance a degradation of the scan result and an increase of measurement error can be observed with a maximum error of 41 μm. In addition, the measured distance shows a higher fluctuation on areas of constant height. Figure 9d (bottom) shows the measurement result for a 5 degree tilt of the sample xy-plane. For illustration the tilt is corrected, however, without initial repositioning the tilt leads to an apparent elongation and a lateral error of several hundred micrometer.

In summary it is shown that the designed robotic inline measurement system, together with the intelligent alignment and measurement process enables high resolution measurements on the single micrometer scale and an efficient operation, with shorter measurement time and a significantly smaller error compared to conventional operation without intelligent alignment.

Post-print version of the article: C. Naverschnigg, E. Csencsics, and G. Schitter, "Flexible Robot-Based In-Line Measurement System for High-Precision Optical Surface Inspection," *IEEE Transactions on Instrumentation and Measurement*, vol. 71, 2022. DOI: 10.1109/TIM.2022.3216680

V. Conclusion

A robot-based in-line measurement system has been designed based on a dual-stage approach, integrating an industrial robot arm to provide flexibility for the inspection of complex shapes within a large working volume and stepper-motor-based linear stages, to perform a high-precision scanning motion. Compared to the state of the art, this setup enables flexible surface inspection and 3D-imaging, with adjustable scanning trajectories and without the limitation of a fixed measurement area. The usage of optical inspection systems, such as triangulation sensors, that exceed the resolution of camera based systems by a factor of 10 and more provide high resolution measurements. Lissajous trajectories and a feature detection algorithm are used to provide a robust measurement process for samples of varying dimensions and to compensate for manufacturing tolerances. For a measurement volume of $51\,\text{mm} \times 51\,\text{mm} \times 25\,\text{mm}$ the robot-based in-line measurement system achieves an axial resolution of $0.385\,\mu\text{m}$, a lateral resolution of $50\,\mu\text{m}$. The total uncertainty for the measurement process equals $6.4\,\mu\text{m}$ at 2σ. The comparison to a reference scan performed by a CMM shows a mean absolute error of $4.4\,\mu\text{m}$. The system accuracy is evaluated to $2.2\,\mu\text{m}$ with a combined standard uncertainty of $1.2\,\mu\text{m}$, exceeding the accuracy of commercially available stereo vision systems by a factor of at least 1.5 [8], [9], and the accuracy of reported robot-based measurement systems by a factor of at least 5 [16]–[20], considering a coverage factor of 2 for the expanded uncertainty. By following the proposed alignment procedure, the data of a coarse Lissajous scan can be used to utilize the maximum possible resolution of an optical measurement system by optimally aligning the measurement system mounted on the robot flange, within an uncertainty mainly determined by the accuracy and repeatability of the robot arm, leading to an improvement of the measurement result and reduction of the measurement error. Therefore, the feature detection and alignment procedure exceeds the accuracy of camera-based systems by a factor of more than 100 [25], [26]. By considering the task of surface inspection of spot welds, a typical spot weld with a diameter of $4\,\text{mm}$ can be located within an average time of $0.75\,\text{s}$, within an area of $20\,\text{mm} \times 20\,\text{mm}$ and can be scanned with the maximum lateral resolution of $50\,\mu\text{m}$ within $3.5\,\text{s}$. The functionality of the system can be extended by integrating additional sensor systems (e.g. laser-ultrasound) to provide subsurface defect characterization of weld spots or other arbitrary point wise sensing systems.

References

[1] D. Imkamp, R. Schmitt, and J. Berthold, “Blick in die Zukunft der Fertigungsmesstechnik,” *Technisches Messen*, vol. 79, no. 10, pp. 433–439, 2012.

[2] D. Imkamp, J. Berthold, M. Heizmann, K. Kniel, M. Peterek, R. Schmitt, J. Seidler, and K.-D. Sommer, “Herausforderungen und Trends in der Fertigungsmesstechnik–Industrie 4.0,” *Tm-Technisches Messen*, vol. 83, no. 7-8, pp. 417–429, 2016.

[3] T.-F. Yao, A. Duenner, and M. Cullinan, “In-line metrology of nanoscale features in semiconductor manufacturing systems,” *Precision Engineering*, vol. 47, pp. 147–157, 2017.

[4] O. Semeniuta, S. Dransfeld, and P. Falkman, “Vision-based robotic system for picking and inspection of small automotive components,” in *2016 IEEE International Conference on Automation Science and Engineering (CASE)*. IEEE, 2016, pp. 549–554.

[5] M. Liebens, A. Jourdain, J. De Vos, T. Vandeweyer, A. Miller, E. Beyne, S. Li, G. Bast, M. Stoerring, S. Hiebert *et al.*, “In-line metrology for characterization and control of extreme wafer thinning of bonded wafers,” in *2017 28th Annual SEMI Advanced Semiconductor Manufacturing Conference (ASMC)*. IEEE, 2017, pp. 331–336.

[6] Z. G. Wu, C. Y. Lin, H. W. Chang, and P. T. Lin, “Inline inspection with an industrial robot (IIIR) for mass-customization production line,” *Sensors (Switzerland)*, vol. 20, no. 11, 2020.

[7] H. Lerchenmüller, T. Selke, and G. Anderson, *Marktstudie 3-D-Messtechnik in der deutschen Automobil-und Zulieferindustrie*. Fraunhofer-Allianz Vision, 2004.

[8] LMI Technologies Inc., “Automatisierung. Inspektion. Optimierung. Gocator, Snapshot Sensoren,” https://lmi3d.com/family/snapshot-sensors/, 2020, accessed: 2021-07-13.

[9] Keyence Corporation, “Inline-3D-Prüfung,” https://www.keyence.de/products/vision/vision-sys/3d_vision/, accessed: 2022-03-10.

[10] W. Gao, H. Haitjema, F. Z. Fang, R. K. Leach, C. F. Cheung, E. Savio, and J. M. Linares, “On-machine and in-process surface metrology for precision manufacturing,” *CIRP Annals*, vol. 68, no. 2, pp. 843–866, 2019. [Online]. Available: https://doi.org/10.1016/j.cirp.2019.05.005

[11] J. Schlarp, E. Csencsics, and G. Schitter, “Optical scanning of a laser triangulation sensor for 3-d imaging,” *IEEE Transactions on Instrumentation and Measurement*, vol. 69, no. 6, pp. 3606–3613, 2019.

[12] V. K. Pathak and A. K. Singh, “Optimization of morphological process parameters in contactless laser scanning system using modified particle swarm algorithm,” *Measurement: Journal of the International Measurement Confederation*, vol. 109, pp. 27–35, 2017. [Online]. Available: http://dx.doi.org/10.1016/j.measurement.2017.05.049

[13] Y. Shimizu, L. C. Chen, D. W. Kim, X. Chen, X. Li, and H. Matsukuma, “An insight into optical metrology in manufacturing,” *Measurement Science and Technology*, vol. 32, no. 4, 2021.

[14] “Kuka AG, Industrieroboter von KUKA,” https://www.kuka.com/en-de/products/robot-systems/industrial-robots, accessed: 2021-06-15.

[15] “ABB AG, ABB Robotics,” https://new.abb.com/products/robotics/de, accessed: 2020-30-12.

[16] S. Yin, Y. Ren, Y. Guo, J. Zhu, S. Yang, and S. Ye, “Development and calibration of an integrated 3D scanning system for high-accuracy large-scale metrology,” *Measurement: Journal of the International Measurement Confederation*, vol. 54, pp. 65–76, 2014. [Online]. Available: http://dx.doi.org/10.1016/j.measurement.2014.04.009

[17] T. Al Khawli, M. Anwar, D. Gan, and S. Islam, “Integrating laser profile sensor to an industrial robotic arm for improving quality inspection in manufacturing processes,” *Proceedings of the Institution of Mechanical Engineers, Part C: Journal of Mechanical Engineering Science*, vol. 235, no. 1, pp. 4–17, 2021.

[18] Z. Fei, X. Zhou, X. Gao, and G. Zhang, “A flexible 3D laser scanning system using a robotic arm,” *Optical Measurement Systems for Industrial Inspection X*, vol. 10329, p. 103294U, 2017.

[19] C. Yu, X. Chen, and J. Xi, “Modeling and calibration of a novel one-mirror galvanometric laser scanner,” *Sensors (Switzerland)*, vol. 17, no. 1, 2017.

[20] ABB AG, ABB Robotics, “3D-Messtechnik für die Qualitätskontrolle,” https://new.abb.com/products/robotics/de/fertigungszellen/3dqi, accessed: 2022-03-10.

[21] D. Wertjanz, T. Kern, E. Csencsics, G. Stadler, and G. Schitter, “Compact scanning confocal chromatic sensor enabling precision 3-D measurements,” *Applied Optics*, vol. 60, no. 25, p. 7511, 2021.

[22] D. Wertjanz, E. Csencsics, T. Kern, and G. Schitter, “Bringing the lab to the fab: Robot-based inline measurement system for precise 3D surface inspection in vibrational environments,” *IEEE Transactions on Industrial Electronics*, vol. 0046, no. c, pp. 1–1, 2022.

[23] R. Söderberg, K. Wärmefjord, L. Lindkvist, and R. Berlin, “The influence of spot weld position variation on geometrical quality,” *CIRP annals*, vol. 61, no. 1, pp. 13–16, 2012.

[24] C. Mineo, C. MacLeod, M. Morozov, S. G. Pierce, R. Summan, T. Rodden, D. Kahani, J. Powell, P. McCubbin, C. McCubbin, G. Munro, S. Paton, and D. Watson, “Flexible integration of robotics, ultrasonics and metrology for the inspection of aerospace components,” *AIP Conference Proceedings*, vol. 1806, no. February 2017, 2017.

[25] A. Khan, C. Mineo, G. Dobie, C. N. Macleod, and S. G. Pierce, “Introducing adaptive vision-guided robotic non-destructive inspection,” pp. 3–5, 2019.

[26] P. L. Inspection, “Production Line Inspection,” pp. 1–19, 2021.

Post-print version of the article: C. Naverschnigg, E. Csencsics, and G. Schitter, “Flexible Robot-Based In-Line Measurement System for High-Precision Optical Surface Inspection,” *IEEE Transactions on Instrumentation and Measurement*, vol. 71, 2022. DOI: 10.1109/TIM.2022.3216680

[27] P. Lardeur, E. Lacouture, and E. Blain, "Spot weld modelling techniques and performances of finite element models for the vibrational behaviour of automotive structures," in *Proceedings of the international seminar on modal analysis*, vol. 1. KU Leuven; 1998, 2001, pp. 387–394.

[28] Physik Instrumente GmbH& Co.KG, "XY Stages," https://www.physikinstrumente.com/en/products/xy-stages/, accessed: 2021-06-25.

[29] Zaber Technologies Inc., "XY, XYZ & Gantry Stages," https://www.zaber.com/products/xy-xyz-gantry-systems, accessed: 2021-06-25.

[30] E. Csencsics and G. Schitter, "System design and control of a resonant fast steering mirror for lissajous-based scanning," *IEEE/ASME Transactions on Mechatronics*, vol. 22, no. 5, pp. 1963–1972, 2017.

[31] K. Deep, K. P. Singh, M. L. Kansal, and C. Mohan, "A real coded genetic algorithm for solving integer and mixed integer optimization problems," *Applied Mathematics and Computation*, vol. 212, no. 2, pp. 505–518, 2009. [Online]. Available: http://dx.doi.org/10.1016/j.amc.2009.02.044

[32] T. Tuma, J. Lygeros, A. Sebastian, and A. Pantazi, "Optimal scan trajectories for high-speed scanning probe microscopy," in *2012 American Control Conference (ACC)*. IEEE, 2012, pp. 3791–3796.

[33] J. Canny, "A computational approach to edge detection," *IEEE Transactions on pattern analysis and machine intelligence*, no. 6, pp. 679–698, 1986.

[34] R. Szeliski, *Computer vision: algorithms and applications*. Springer Science & Business Media, 2010.

[35] M. A. Fischler and R. C. Bolles, "Random sample consensus: a paradigm for model fitting with applications to image analysis and automated cartography," *Communications of the ACM*, vol. 24, no. 6, pp. 381–395, 1981.

[36] E. B. Dam, M. Koch, and M. Lillholm, *Quaternions, interpolation and animation*. Citeseer, 1998, vol. 2.

[37] DIN EN ISO 18595:2021, "Resistance welding - Spot welding of aluminium and aluminium alloys - Weldability, welding and testing," International Organization for Standardization, Geneva, CH, Standard, May 2021.

[38] T. seven orgonlzatiarls Supportedthe, "Guide to the expression of uncertainty in measurement," 1995.

[39] A. M. Müller, D. Schubert, D. Drummer, and T. Hausotte, "Determination of the single point uncertainty of customized polymer gear wheels using structured-light scanning with various polygonization settings," *Journal of Sensors and Sensor Systems*, vol. 9, no. 1, pp. 51–60, 2020.

[40] C. Haider, "Coordinate measuring machine for simultaneous double-sided optical surface metrology using a confocal chromatic sensor," Master thesis, Technical university of Vienna, 2020.

[41] P. J. Besl and N. D. McKay, "Method for registration of 3-d shapes," in *Sensor fusion IV: control paradigms and data structures*, vol. 1611. International Society for Optics and Photonics, 1992, pp. 586–606.

[42] J. H. Friedman, J. L. Bentley, and R. A. Finkel, "An algorithm for finding best matches in logarithmic expected time," *ACM Transactions on Mathematical Software (TOMS)*, vol. 3, no. 3, pp. 209–226, 1977.

Christopher Naverschnigg is currently Doctoral Researcher with the Automation and Control Institute (ACIN), TU Wien, Vienna, Austria. He received the M.Sc. degree in electrical engineering from TU Wien, Vienna, Austria in 2021.
His primary research interests are in-line metrology and modelling and control of mechatronic systems, especially high-performance telescope systems for object tracking.

Ernst Csencsics is Assistant Professor for Measurement Systems at the Automation and Control Institute (ACIN) of TU Wien. He received an MSc. and a PhD degree (sub auspiciis) in Electrical Engineering from TU Vienna, Austria in 2014 and 2017, respectively.
His primary research interests are on high performance mechatronic systems, the development of holistic methods for multidisciplinary system design and integration, opto-mechatronic measurement and imaging systems, precision engineering, and robot-based in-line measurement systems. He received the journal best paper award of *IEEE/ASME Transactions on Mechatronics* (2018), the best paper award at the *IEEE International Instrumentation and Measurement Technology Conference* (2022) and the best student paper award at the *American Control Conference* (2016).

Georg Schitter (Senior Member, *IEEE*) received the B.Sc. degree in electrical engineering from TU Graz, Graz, Austria, in 2000, and the M.Sc. degree in information technology, and Ph.D. degrees in control engineering and nanotechnology from ETH Zurich, Zurich, Switzerland, in 2004.
He is Professor for Advanced Mechatronic Systems with the Automation and Control Institute (ACIN), TU Wien. His primary research interests are on high-performance mechatronic systems, particularly for applications in the high-tech industry, scientific instrumentation, and mechatronic imaging systems, such as AFM, scanning laser and LIDAR systems, telescope systems, adaptive optics, and lithography systems for semiconductor industry. Prof. Schitter was the recipient of the Journal Best Paper Award of *IEEE/ASME Transactions on Mechatronics* (2018), of the *IFAC Mechatronics* (2008–2010), of the *Asian Journal of Control* (2004–2005), and the 2013 *IFAC Mechatronics Young Researcher Award*. He was an Associate Editor for *IFAC Mechatronics, Control Engineering Practice*, and for the *IEEE TRANSACTIONS ON MECHATRONICS*.

Post-print version of the article: C. Naverschnigg, E. Csencsics, and G. Schitter, "Flexible Robot-Based In-Line Measurement System for High-Precision Optical Surface Inspection," *IEEE Transactions on Instrumentation and Measurement*, vol. 71, 2022. DOI: 10.1109/TIM.2022.3216680